Developmental Cell *10*, 743–757, June, 2006 ©2006 Elsevier Inc. DOI 10.1016/j.devcel.2006.04.007

C. elegans Dynamin Mediates the Signaling of Phagocytic Receptor CED-1 for the Engulfment and Degradation of Apoptotic Cells

Xiaomeng Yu,[1] Sampeter Odera,[1] Chin-Hua Chuang,[1] Nan Lu,[1] and Zheng Zhou[1,2,*]

[1] Verna and Marrs McLean Department of Biochemistry and Molecular Biology

[2] Program in Developmental Biology

Baylor College of Medicine

Houston, Texas 77030

Summary

Dynamins are large GTPases that act in multiple vesicular trafficking events. We identified 14 loss-of-function alleles of the *C. elegans* dynamin gene, *dyn-1,* that are defective in the removal of apoptotic cells. *dyn-1* functions in engulfing cells to control the internalization and degradation of apoptotic cells. *dyn-1* acts in the genetic pathway composed of *ced-7* (ABC transporter), *ced-1* (phagocytic receptor), and *ced-6* (CED-1's adaptor). DYN-1 transiently accumulates to the surface of pseudopods in a manner dependent on *ced-1*, *ced-6*, and *ced-7*, but not on *ced-5*, *ced-10*, or *ced-12*. Abnormal vesicle structures accumulate in engulfing cells upon *dyn-1* inactivation. *dyn-1* and *ced-1* mutations block the recruitment of intracellular vesicles to pseudopods and phagosomes. We propose that DYN-1 mediates the signaling of the CED-1 pathway by organizing an intracellular vesicle pool and promoting vesicle delivery to phagocytic cups and phagosomes to support pseudopod extension and apoptotic cell degradation.

Introduction

Animal cells undergoing programmed cell death (apoptosis) are rapidly engulfed (phagocytosed) and degraded by other cells. The efficient removal of apoptotic cells facilitates organ sculpting and tissue remodeling. Furthermore, it prevents tissue injury and inflammatory and autoimmune responses (reviewed by Savill and Fadok, 2000). In addition, engulfing cells can assist in the suicide of apoptotic cells (reviewed by Reddien and Horvitz, 2004).

During the development of *Caenorhabditis elegans* hermaphrodites, 131 somatic cells and ~500 germ cells undergo programmed cell death and are rapidly removed (Sulston and Horvitz, 1977; Sulston et al., 1983; Gumienny et al., 1999). In *C. elegans*, engulfing cells produce thin cytoplasmic extensions (pseudopods) to embrace dying cells, as in other metazoans; however, dying cells are engulfed by neighboring cells rather than by professional phagocytes such as macrophages in mammals (reviewed by Zhou et al., 2004). Hypodermal cells, which are large and contact many apoptotic cells, are the major engulfing cells for somatic apoptotic cells during embryonic and larval development. Pharyngeal muscles and intestinal cells can also engulf somatic apoptotic cells in embryos. Gonadal sheath cells engulf all apoptotic germ cells (reviewed by Zhou et al., 2004).

Seven *C. elegans* genes—*ced-1* (cell death abnormal), *ced-2*, *ced-5*, *ced-6*, *ced-7*, *ced-10*, and *ced-12*—have been identified from analyses of viable mutants containing persistent apoptotic cells, referred to as cell corpses (reviewed by Zhou et al., 2004). Cell corpses can be distinguished as highly refractile discs under a Nomarski differential interference contrast (DIC) microscope. Genetic and molecular studies indicate that six of these genes act in two partially redundant pathways to control cell corpse engulfment (Ellis et al., 1991; Mangahas and Zhou, 2005). One, or possibly both, of these pathways acts through the small Rac GTPase CED-10 (Kinchen et al., 2005; Mangahas and Zhou, 2005). In one pathway, CED-2/CrkII, CED-5/Dock180, and CED-12/ELMO1 act together to regulate CED-10, which, in turn, promotes cytoskeletal reorganization during engulfment (reviewed by Zhou et al., 2004).

CED-1, CED-6, and CED-7 act in the other pathway. The phagocytic receptor CED-1 is a single-pass transmembrane protein with a large extracellular domain that recognizes cell corpses and a short intracellular domain required for downstream signaling (Zhou et al., 2001b). CED-1 activity is required in engulfing cells, but not in cells destined to die (Zhou et al., 2001b). CED-1 clusters to the region of the engulfing cell membrane in contact with cell corpses and initiates engulfment. Although the ligand for CED-1 has not been identified, phosphatidylserine has been proposed as a candidate (Zhou et al., 2001b). CED-7, a homolog of mammalian ABC transporters (Wu and Horvitz, 1998a), is required for CED-1 clustering and is implicated in presenting the CED-1 ligand on the surface of apoptotic cells (Zhou et al., 2001b). CED-6 contains a phosphotyrosine binding (PTB) domain (Liu and Hengartner, 1998) and appears to act downstream of CED-1 (Zhou et al., 2001b). In heterologous systems, the PTB domain of CED-6 was reported to interact with the intracellular domain of CED-1 (Su et al., 2002).

The removal of apoptotic cells requires the activation of multiple cellular processes in engulfing cells, including actin cytoskeleton rearrangement, membrane extension, membrane enclosure, and the delivery of digestive enzymes to phagosomes. Recently, it was reported that the CED-1 pathway regulates actin polymerization in cells engulfing germ cell corpses (Kinchen et al., 2005). Despite the likely involvement of dozens of proteins, previous genetic screens for viable engulfment mutants have not identified many genes directly involved in the cellular events mentioned above (reviewed by Zhou et al., 2004). Although engulfment per se is not essential for *C. elegans* development (Ellis et al., 1991), null mutants of *ced-10* display maternal-effect embryonic lethality (Lundquist et al., 2001), indicating that there exist additional genes with separate functions required for engulfment and for development. This class of genes was likely missed in previous screens. We undertook genetic screens to recover lethal mutants containing persistent cell corpses and have identified 14

*Correspondence: zhengz@bcm.tmc.edu

loss-of-function alleles in *dyn-1*, which encodes the *C. elegans* homolog of dynamin. Our study suggests that DYN-1 acts to promote vesicle recruitment and fusion to extending pseudopods and maturing phagosomes in response to CED-1 signaling.

Results

We Isolated 14 Mutant Alleles of *C. elegans dyn-1* that Contain Many Persistent Cell Corpses and Are Embryonic Lethal

The *n4039* mutant was isolated in a screen for mutants that, as homozygotes, arrest during embryonic development and contain persistent cell corpses (Z.Z. and H.R. Horvitz, unpublished data). By the 4-fold stage of embryogenesis, all 113 apoptotic cells in a wild-type embryo have been removed due to rapid engulfment and degradation (Ellis et al., 1991). In contrast, *n4039* homozygous mutant embryos descended from *n4039*/+ heterozygous mothers contain a large number of cell corpse-like objects (Figures 1B and 2B). The zygotic embryonic lethal (Emb) phenotype and the presence of persistent cell corpses (Ced) phenotype associated with *n4039* are both recessive, 100% penetrant, and cosegregate with each other (Figure 1B and data not shown), indicating that *n4039* is a loss-of-function mutation that causes both of these phenotypes.

We cloned the gene whose mutation results in the Emb and Ced phenotypes observed in *n4039* animals (see the Supplemental Data including Figure S1, available with this article online). This gene, *dyn-1*, encodes a protein homologous to dynamins, a family of large GTPases that regulate vesicle transport events (Clark et al., 1997) (Figure 1A). A total of 13 additional Emb and Ced mutants that we isolated (Z.Z. and H.R. Horvitz, S.O., and Z.Z., unpublished data) are also mutant alleles of *dyn-1* (Supplemental Data). With the exception of *en9* (I401F), all remaining alleles of *dyn-1* bear missense mutations in the GTPase domain essential for the function of mammalian and *Drosophila* dynamins (reviewed by Hinshaw, 2000) (Figure 1A). Mutations in the GTPase domain are located in conserved motifs important for GTP binding, conformational changes between the GDP and GTP bound states, or structural integrity of the GTPase domain (Figure S2) (Niemann et al., 2001). A number of these mutations cause a strong Ced phenotype (Figure 1B), suggesting that the GTPase domain of DYN-1 might be important for the removal of apoptotic cells.

We found that the cDNAs encoding each of the two splice variants (*a* and *b*) of *dyn-1* expressed under the control of a 3.5 kb P_{dyn-1} promoter efficiently rescued the Ced phenotype of *dyn-1(n4039)* mutants, with or without a C-terminal *gfp* fusion (Figure 1C, X.Y. and Z.Z., unpublished data). We thus used variant *a* cDNA for all further experiments. We also found that the expression of a cDNA encoding the ubiquitously expressed human dynamin 2 (Hinshaw, 2000) in *C. elegans* under the control of P_{dyn-1} resulted in a 57% reduction in the number of persistent cell corpses in *dyn-1(n4039)* mutant embryos (Figure 1C). This result indicates that human dynamin 2 can perform functions similar to DYN-1 in the removal of *C. elegans* cell corpses, albeit less efficiently.

Two *dyn-1* Mutant Alleles Isolated by Others Do Not Display an Obvious Ced Phenotype

dyn-1(tm852) is a deletion allele that eliminates residues 316–838 of DYN-1 (Figure 1A) (S. Mitani, personal communication). We found that the *tm852* homozygous embryos produced by *tm852*/+ mothers did not contain extra cell corpses, and that they hatched into L1 larvae but failed to develop further (Figure 1B). RNA interference (RNAi) inactivation of *dyn-1* leads to a strong Ced phenotype and, primarily, early embryonic arrest (Supplemental Data and Figure S1C). Compared to *dyn-1*(RNAi), the *tm852* mutation affects later stages of development, suggesting that this mutation results in a partial loss of *dyn-1* function. *dyn-1(ky51)*, a viable, temperature-sensitive allele that displays severe defects in the recycling of synaptic vesicles, the endocytosis of yolk into oocytes, and fluid phase endocytosis by the scavenger coelomocytes at 25ºC, the restrictive temperature (Clark et al., 1997; Grant and Hirsh, 1999; Fares and Greenwald, 2001), displays an extremely weak and partially penetrant Ced phenotype at 25ºC (Figure 1B). These results indicate that the removal of apoptotic cells is a unique aspect of *dyn-1* function severely affected by the Ced alleles we isolated, yet weakly or not affected by the *ky51* or *tm852* mutation.

Cell Corpses Persist in *dyn-1* Mutants Due to Defects in Cell Corpse Removal Rather than Abnormal Apoptosis or Developmental Defects

The *ced-3(n717)* mutation inactivates the CED-3 caspase and blocks all programmed cell deaths (Yuan et al., 1993). In contrast to *dyn-1(n4039)* embryos, no cell corpse-like objects were observed in *ced-3(n717); dyn-1(n4039)* double mutants (Figures 2A and 2B, [f]), indicating that the observed cell corpse-like objects are indeed cell corpses.

The majority (109 of 113) of normal embryonic cell deaths occur during mid-embryogenesis, within a period 200–460 min after the first cleavage (cytokinesis) of a fertilized egg (Sulston et al., 1983). We observed similar numbers of cell corpses in *dyn-1(n4039)* and wild-type embryos at the comma stage (Figures 2C and 2F). As development continues, the number of cell corpses increases in *dyn-1(n4039)* embryos but steadily decreases in wild-type embryos (Figure 2C). To determine whether apoptotic cells persist for longer periods in *dyn-1(n4039)* mutants, we measured the duration of individual cell corpses distinguished under a DIC microscope by using time-lapse recording (Experimental Procedures). In wild-type embryos, the majority (80.9%) of cell corpses disappeared within 30 min, and no cell corpse lasted longer than 50 min (Figure 2D). In *dyn-1(n4039)* embryos, however, only 40% of the cell corpses disappeared within 30 min; 40% persisted longer than 60 min. A similar distribution of cell corpse duration was observed among *ced-1(e1735)* embryos (Figure 2D). A number of cell corpses present in late 4-fold-stage *dyn-1(n4039)* embryos persisted for longer than 24 hr (Figure 2B, [e]). These observations indicate that *dyn-1(n4039)* embryos are defective in removing cell corpses.

Next, we determined whether programmed cell death events are affected by the *dyn-1(n4039)* mutation. Using time-lapse recording (Experimental Procedures), we found that during the period of 200–400 min past the first

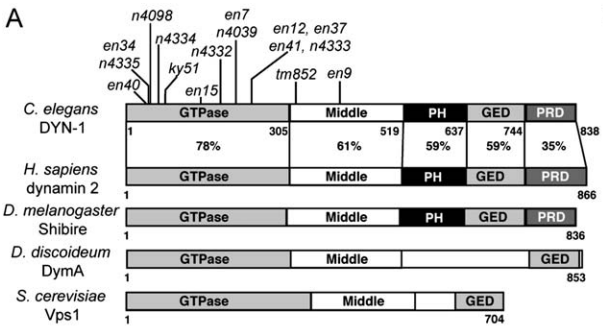

B

Allele name	Nucleotide and amino acid changes	Codon position	No. of cell corpses	Embryonic lethality
en40	GGA (G) to GAA (E)	40	28.5 ± 2.4	100%
en34, n4335	TCC (S) to TTC (F)	43	26.3 ± 4.0	100%
n4098	GGA (G) to GAA (E)	45	30.7 ± 3.9	100%
n4334	GGA (G) to GAA (E)	62	5.9 ± 1.9	100%
en15	CCC (P) to CTC (L)	146	12.6 ± 1.8	100%
n4332	CCG (P) to CTG (L)	178	12.9 ± 3.8	100%
n4039	GGA (G) to GAA (E)	204	25.8 ± 3.7	100%
en7	GGA (G) to AGA (R)	204	16.8 ± 3.4	100%
en37, en41, n4333	GGA (G) to GAA (E)	235	24.3 ± 3.4	100%
en12	GGA (G) to AGA (R)	235	24.8 ± 2.5	100%
en9	ATC (I) to TTC (F)	401	26.1 ± 4.4	100%
ky51 at 20°C	CCA (P) to TCA (S)[a]	70	0.1 ± 0.3	1%
ky51 at 25°C	CCA (P) to TCA (S)	70	3.8 ± 2.4[b]	24%
tm852	Deletion	316-838	0.1 ± 0.3	0%[c]
wild-type	NA	NA	0.2 ± 0.4	0%

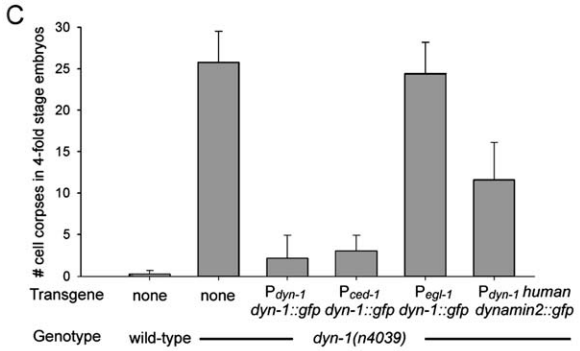

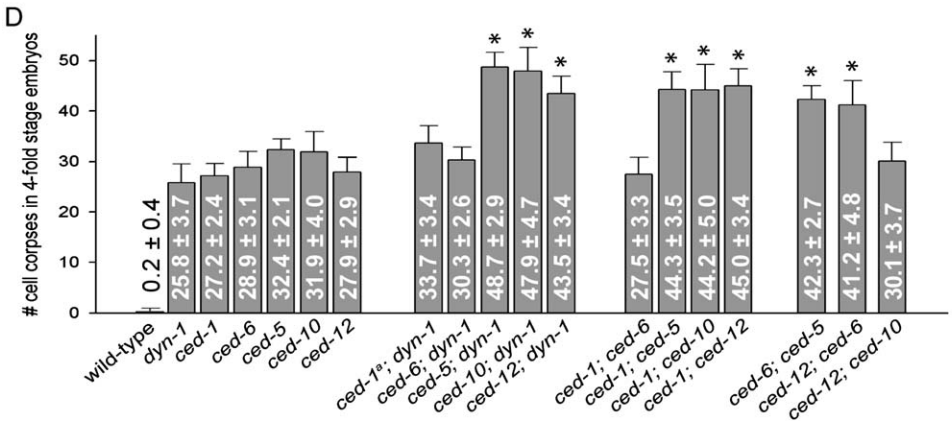

Figure 1. A Total of 14 Mutant Alleles of *dyn-1* Have the Ced and Emb Phenotypes, and *dyn-1* Acts in Engulfing Cells in the *ced-1* Pathway for the Removal of Cell Corpses

(A) Domain structure of dynamins. The locations of *dyn-1* mutations are indicated. The percent amino acid identity of each domain between DYN-1 and human dynamin 2 is indicated. PH, pleckstrin-homology domain; GED, GTPase-effector domain; PRD, proline-rich domain.

(B) Molecular lesions and quantitative mutant phenotypes of *dyn-1* mutants. Except for *ky51* and wild-type embryos, homozygous embryos were generated from heterozygous mothers. For each mutant, 15 late 4-fold-stage embryos were scored, and data are presented as mean ± standard deviation (SD). [a]Clark et al., (1997). [b]Only embryos that contained > 1 cell corpse (22% of all embryos examined) were scored. [c]*tm852* animals are 100% L1 larvae arrest.

(C) Number of cell corpses in late 4-fold-stage embryos of different genotypes that express different transgenes. The number of embryos scored for each sample > 12. Error bars represent standard deviations.

(D) Number of cell corpses in 4-fold-stage single and double mutant embryos (x axis: genotypes). Alleles used are: *dyn-1(n4039)*, *ced-1(e1735)*, *ced-6(n2095)*, *ced-5(n1812)*, *ced-10(n3246)*, *ced-12(n3261)*, and *ced-1(n1506)* (29.8 ± 3.2 cell corpses as single mutants, only used in *ced-1(n1506)*[a]*; dyn-1(n4039)*). The number of animals scored for each genotype is > 10. Numeric datum is shown inside each bar. Asterisks mark double mutants that contain significantly more cell corpses than each single mutant. Error bars represent standard deviations.

cleavage, the number of cell death events in the entire *dyn-1(n4039)* embryo as well as the timing that each cell death occurred were similar to those in wild-type embryos (Figure 2E). These results indicate that the *dyn-1(n4039)* mutation does not affect the number or the developmental timing of programmed cell death events. Thus, the increased number of cell corpses in the *dyn-1(n4039)* embryo is solely due to the failure of cell corpse removal, not to the increased incidence of apoptosis.

Maternal and Zygotic Contribution of *dyn-1*

dyn-1(n4039) homozygous embryos produced by *dyn-1(n4039)/+* mothers apparently develop normally before reaching the 4-fold stage, judging by body elongation, body movement, and the development of pharynges and intestinal tracts (Figure 2F), indicating that the *n4039* mutation does not significantly affect early- and mid-stage embryogenesis. Mutant animals fail to hatch and arrest at the late 4-fold stage, when they gradually

A

Genotype	# cell corpses in 4-fold embryos
wild-type	0.3 ± 0.4 (n=50)
n4039	25.8 ± 3.7 (n=15)
ced-3	0.1 ± 0.1 (n=50)
ced-3; n4039	0.1 ± 0.1 (n=50)

Genotype of P0	Total progeny	Dead eggs	Dead/total
n4039/+	403	97	24.1%
ced-3; n4039/+	441	114	25.9%

B

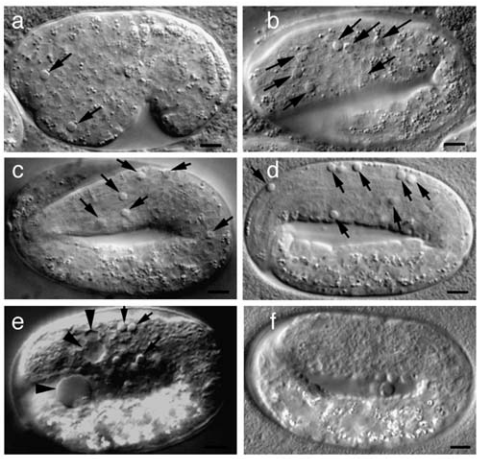

C

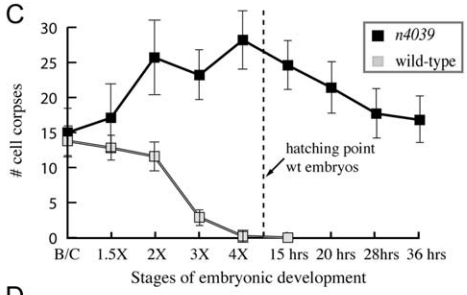

D

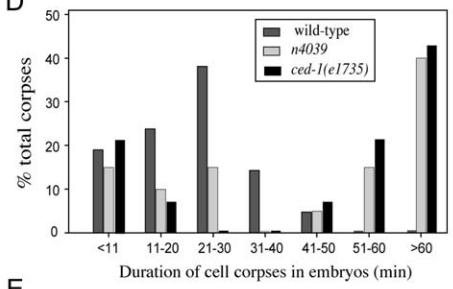

E

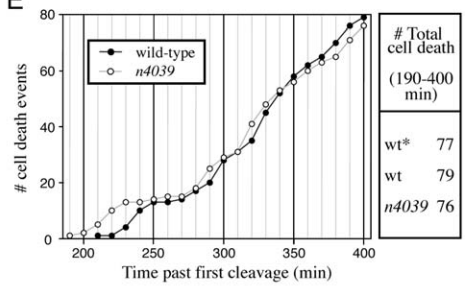

F

Stages embryonic development	Time entering each stage (after first cleavage) wt (Sulston et al. 1983)	wt (our observation)	*n4039*
comma	~380 min	376 ± 10 min	381 ± 11 min
1.5-fold	~420 min	417 ± 8 min	425 ± 2 min
2-fold	~460 min	445 ± 10 min	446 ± 4 min
3-fold	~520 min	502 ± 18 min	504 ± 16 min
4-fold	ND	605 ± 14 min	615 ± 11 min
hatching	~800 min	771 ± 15 min	Not observed
Other Landmarks			
Period forming pharyngeal grinder	ND	605 - 664 min	615 - 685 min
Body movement	2-fold - hatching	2-fold - hatching	2-fold - > 800 min
Pharyngeal pumping	~767 min	741 ± 15 min	Not observed

Figure 2. *dyn-1(n4039)* Mutant Phenotypes

(A) Eggs that failed to hatch 24 hr after being laid are considered dead. n, number of embryos scored.

(B) Nomarski DIC images of *n4039* embryos. Anterior is to the left. The scale bar is 5 μm. Arrows indicate cell corpses. (a–d) *n4039* embryos at comma, 2-fold, 3-fold, and 4-fold stages, respectively. (e) An *n4039* embryo 24 hr after the late 4-fold stage. Arrowheads indicate vacuoles. (f) A *ced-3(n717); n4039* embryo past the late 4-fold stage. No cell corpses are visible.

(C) The numbers of cell corpses in wild-type and *n4039* mutant embryos at different embryonic stages. A total of 15 embryos were scored for each data point. Error bars represent standard deviations. B/C, bean to comma stages; X, fold.

(D) Histograms indicating the distribution of cell corpses (22 analyzed for each genotype) with different duration periods (from <11 min to >60 min, separated into 7 groups).

(E) The total numbers of cell death events occurring between 190–400 min past the first cleavage are plotted in 10 min intervals on the left panel and summed on the right panel. *Sulston et al., (1983).

(F) The process of embryonic development starting at the one-cell stage was recorded for 800 min for wild-type (wt) (n = 12) and *n4039* (n = 5) embryos.

stop moving and display excessive autofluorescence and numerous vacuoles, landmarks of tissue degeneration (Figure 2B, [e] and [f] and Figure 2F). This lethality is not suppressed in *ced-3(n717); dyn-1(n4039)* embryos (Figure 2A), indicating that the failure to remove cell corpses is not the cause of embryonic lethality. The embryonic development phenotypes of the other 13 *dyn-1* alleles are similar to those of *n4039* (data not shown).

We also observed that the reduction of maternal *dyn-1* activity in addition to the loss of zygotic *dyn-1* activity results in the developmental arrest of many embryos at stages earlier than the 4-fold stage (Supplemental Data and Figure S1B). In addition, those embryos that developed to the 4-fold stage contain 51% more cell corpses than *dyn-1(n4039)* embryos produced by *dyn-1(n4039)/+* mothers (Figure S1B). These observations

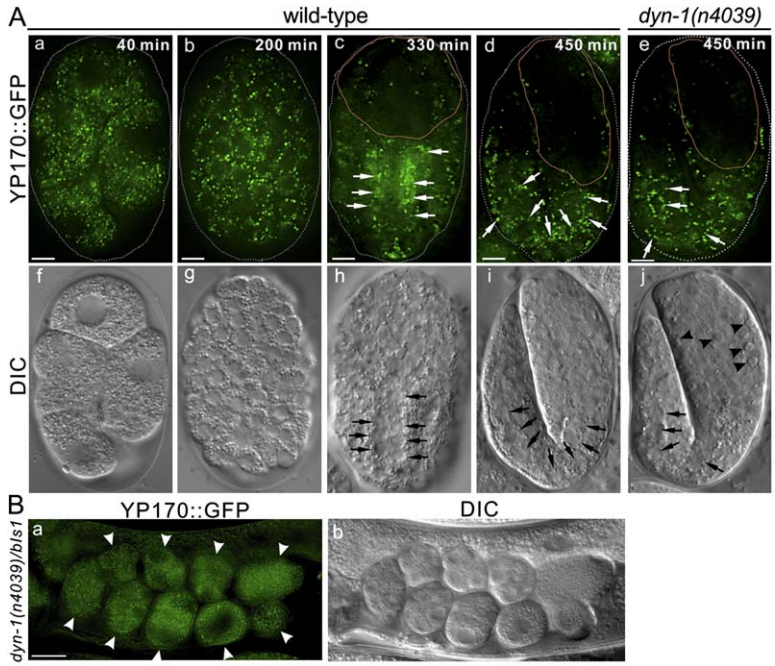

C

Genotype of P0	YP170::GFP-positive progeny	
	%	n
wild-type	100	100
dyn-1(n4039)/+	100	100

Genotype of embryos	Embryos YP170::GFP redistributed	
	%	n
wild-type	100	25
dyn-1(n4039)	100	11

D

Genotype	# Cell corpses	
	20°C	25°C
wild-type	0.2 ± 0.4	0.3 ± 0.5
rme-1(b1045)	0.4 ± 0.6	ND
rme-2(b1008)	0.8 ± 1.2	ND
rme-8(b1023ts)	0.1 ± 0.3	3.1 ± 1.7

Figure 3. The Uptake and Redistribution of Yolk Are Normal in *dyn-1(n4039)* Mutants

(A) (a–d) Epifluorescence images of YP170::GFP in wild-type embryos at different stages (labeled as min past the first cleavage) and in a (e) *dyn-1(n4039)* embryo. (f)–(j) are the DIC images of (a)–(e), respectively. Symbols: black arrows, intestinal precursor cells; white arrows, YP170::GFP spots in intestinal cells; arrowheads, cell corpses; dotted lines, the embryo boundary; solid lines, the head region of embryos. Anterior is to the top. The scale bars are 5 μm.

(B) (a) Epifluorescence and (b) DIC images of the uterus of a *dyn-1(n4039)/bIs1* hermaphrodite that contains embryos (white arrowheads). Ventral is to the bottom. The scale bar is 20 μm.

(C) Frequencies of the presence (upper panel) and redistribution (lower panel) of YP170::GFP in embryos produced by wild-type (*bIs1*) and *dyn-1(n4039)/+* (*dyn-1(n4039)/bIs1*) hermaphrodites. Embryos < 200 min of age (upper panel) or at the 2-fold stage (lower panel) were scored. n, the number of embryos scored.

(D) The number of cell corpses in late 4-fold-stage embryos was scored. For every sample, >15 embryos were scored, and data are presented as mean ± SD. ND, not determined.

suggest that the maternal *dyn-1* product plays additional roles in supporting embryonic development and the removal of apoptotic cells.

The Uptake and Intercellular Redistribution of Yolk Is Normal in *dyn-1* Mutant Embryos

Dynamin plays an essential role in clathrin-mediated endocytosis (reviewed by Hinshaw, 2000). To examine whether the Ced phenotype is an indirect consequence of defects in endocytosis or other vesicle transport events, we characterized the uptake and redistribution of yolk in *dyn-1* mutant embryos. In *C. elegans*, yolk, a lipoprotein complex produced in large quantities by intestinal cells in the mothers and transported to the gonad, is recognized by the receptor RME-2 on the surface of oocytes and internalized into oocytes through clathrin-mediated endocytosis (Grant and Hirsh, 1999). During early- and mid-stage embryos, yolk is secreted from most embryonic cell types, presumably via exocytosis, and internalized into intestinal precursor cells (Bossinger and Schierenberg, 1996). Using a GFP fusion of YP170, a vitellogenin and a component of yolk, Grant and Hirsh (1999) found that the uptake of yolk by oocytes was strongly reduced in *dyn-1*(RNAi) and *dyn-1(ky51)* mutant animals.

Consistent with previous reports (Bossinger and Schierenberg, 1996; Grant and Hirsh, 1999), we observed that maternally produced YP170::GFP from *bIs1*, an integrated array on the X chromosome (Grant and Hirsh, 1999), was internalized by wild-type oocytes and evenly distributed to every cell in early embryos (<200 min old) (Figures 3A and 3B). Afterward, yolk started to accumulate in intestinal cells and diminish from most other cell types (Figure 3A, [c] and [h]). By the 2-fold stage, yolk is strongly enriched in intestinal cells and depleted from the entire head region (Figure 3A, [d] and [i]). In all *dyn-1(n4039)* embryos generated by *dyn-1(n4039)/bIs1* mothers, maternally produced YP170::GFP is internalized and undergoes subsequent redistribution in a pattern identical to wild-type (Figure 3A, [e] and [j] and Figure 3C). These results imply that the defects in the removal of apoptotic cells in *dyn-1(n4039)* embryos are not due to general failure of endocytosis or exocytosis.

We also scored the number of cell corpses in late 4-fold-stage embryos bearing mutations in *rme-1*, *rme-2*, and *rme-8*, three genes required for efficient endocytosis of yolk. Unlike mutations in *rme-2*, which specifically affect the endocytosis of yolk, but like *dyn-1(ky51)*, mutations in *rme-1* and *-8* also result in profound defects in fluid phase endocytosis executed by coelomocytes (Fares and Greenwald, 2001). *rme-1* encodes an endosomal-associated protein containing a conserved EH domain; *rme-8* encodes a J domain protein associated with clathrin-coated pits (Grant et al., 2001; Zhang et al., 2001). No or very few persistent cell corpses were

A

Genotype	# DIC cell corpses/gonad arm		Observation under EM		
	31 hr after L4	48 hr after L4	Engulfed CC	Unengulfed CC	% engulfed/total
dyn-1(RNAi)	23.7 ± 6.2	ND, gonad deformed	21[a]	29[a]	42%
ced-1(e1735)	18.2 ± 5.6	51.8 ± 8.1	0[b]	30[b]	0%
wild-type	1.6 ± 1.5	3.9 ± 1.6	7[b]	0[b]	100%

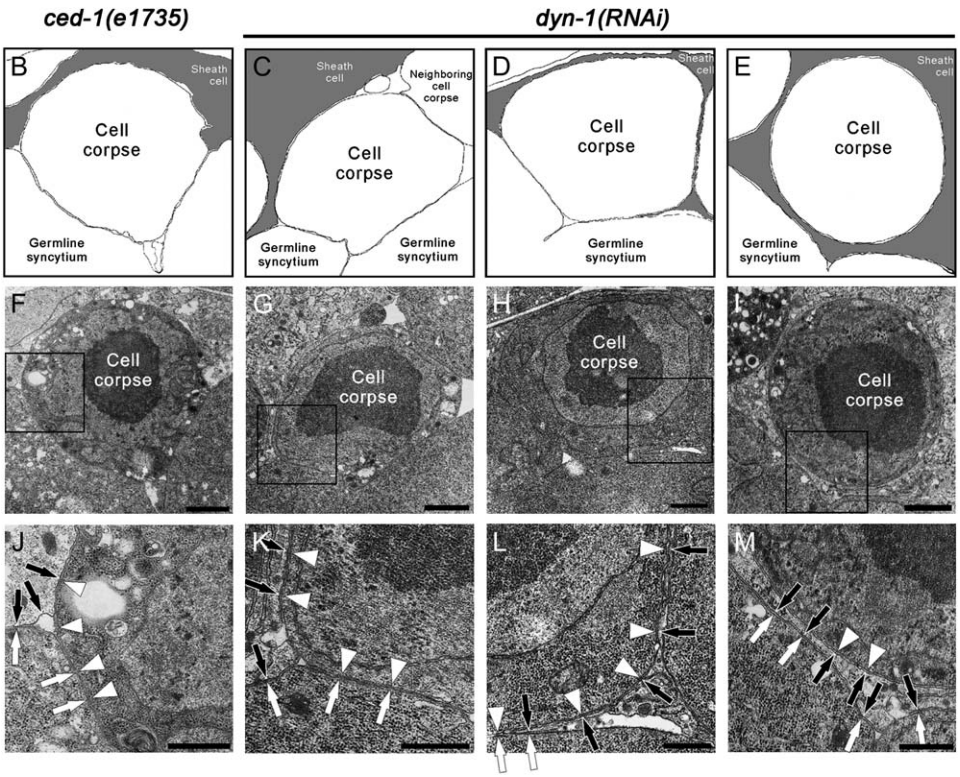

Figure 4. Both the Engulfment and the Degradation of Apoptotic Cells Are Defective in *dyn-1*(RNAi) Animals

(A) The numbers of germ cell corpses per gonad arm were scored from 15 animals of each genotype at 2 time points by using the DIC microscope and were presented as mean ± SD. The EM results are from three, four, and two gonad arms from *dyn-1*(RNAi), *ced-1*, and wild-type animals, respectively, at either [a]31 hr or [b]48 hr past the mid-L4 stage. CC, cell corpse.

(B–M) (F–I) Transmission electron microscopy images of cell corpses and their neighboring cells. The scale bar is 1 μm. Traces of the membranes are shown in (B)–(E). Amplified images corresponding to framed regions in (F)–(I), respectively, are displayed in (J)–(M). The scale bars are 500 nm. Black arrows indicate the membranes of gonadal sheath cells. White arrowheads indicate the membranes of cell corpses. White arrows indicate the membranes of the germline syncytium.

observed in *rme-1*, *-2*, or *-8* mutants (Figure 3D). Thus, endocytosis mediated by *rme-1*, *-2*, and *-8* does not appear to play a major role in the removal of apoptotic cells.

dyn-1 Is Required for Both the Engulfment and Degradation of Apoptotic Cells

The persistent cell corpses observed in *dyn-1* mutant embryos could result from a defect in the engulfment of cell corpses, in the digestion of internalized cell corpses, or in both. We used transmission electron microscopy (TEM) to distinguish among these possibilities. *dyn-1*(RNAi) results in the accumulation of many germ cell corpses in the adult hermaphrodite gonad (Figure 4A). We analyzed these germ cell corpses with TEM (Experimental Procedures) (Figure S3). Germ cell corpses cellularize from the germline syncytium and are engulfed exclusively by gonadal sheath cells, which surround most parts of the germline syncytium (Gumienny et al., 1999). In wild-type gonads, due to the rapid engulfment and degradation of cell corpses, despite a large number of cell death events, only a few cell corpses are visible at any given time (Figure 4A). In contrast, many cell corpses accumulate in adult *ced-1(e1735)* hermaphrodites, and gonadal sheath cells fail to encircle these corpses (Figures 4A, 4B, 4F, and 4J) (Zhou et al., 2001b). Among the 50 germ cell corpses found in 3 gonadal arms treated with *dyn-1*(RNAi), 21 are fully engulfed; however, they remained undigested inside gonadal sheath cells (Figures 4A, 4E, 4I, and 4M). The remaining 29 cell corpses are either partially embraced by pseudopods extended from sheath cells (Figures 4D, 4H, and 4L) or are in contact with sheath cells that do not extend any pseudopod (Figures 4C, 4G, and 4K). These observations indicate that the inactivation of *dyn-1* affects both the internalization and the degradation of germ cell corpses.

DYN-1 Is Expressed and Acts in Engulfing Cells for the Removal of Apoptotic Cells

In larvae and adult hermaphrodites, the expression of a P_{dyn-1} *dyn-1::gfp* reporter was observed in all previously described *dyn-1*-expressing tissues, including gonadal sheath cells (Figure S4, [d]–[e] and data not shown) (Labrousse et al., 1998). In embryos, many cell types express P_{dyn-1} *dyn-1::gfp*, including known engulfing cells such as the hypodermal cells, intestinal precursor cells, and the entire pharyngeal primordium (Figure S4, [a]–[c] and data not shown).

To determine whether DYN-1 activity is required in the engulfing cell or the dying cell for the removal of cell corpses, we expressed *dyn-1* cDNA under the control of the engulfing cell-specific promoter P_{ced-1} or the dying cell-specific promoter P_{egl-1} (Zhou et al., 2001b) and examined the ability of these transgenes to promote engulfment. P_{ced-1} *dyn-1::gfp* rescued the Ced phenotype of *dyn-1(n4039)* to the same extent as P_{dyn-1} *dyn-1cDNA* (Figure 1C). In contrast, P_{egl-1} *dyn-1::gfp* did not exhibit significant rescuing activity, although it produced a GFP signal in dying cells (Figure 1C and data not shown). These results indicate that the *dyn-1* activity in engulfing cells, but not in dying cells, is sufficient for the rescue of the Ced phenotype. *dyn-1* thus primarily functions in engulfing cells for the removal of apoptotic cells.

dyn-1 Acts in the CED-1 Signaling Pathway for the Removal of Cell Corpses

We sought to determine in which of the two partially redundant engulfment pathways *dyn-1* acts. A mutation in an engulfment gene should not enhance the phenotype caused by a null mutation in a gene in the same pathway, but it should enhance the phenotype caused by a null mutation in a gene in a parallel pathway (Reddien and Horvitz, 2004; Mangahas and Zhou, 2005). This epistasis grouping is the basis for concluding that *ced-1*, *-6*, and *-7* act in one pathway, while *ced-2*, *-5*, *-10*, and *-12* act in another. Using the null alleles *ced-1(n1506)* (Z.Z., unpublished data) and *ced-5(n1812)* (Wu and Horvitz, 1998b) and the strong alleles *ced-6(n2095)* (Liu and Hengartner, 1998), *ced-10(n3246)* (Reddien and Horvitz, 2000), and *ced-12(n3261)* (Zhou et al., 2001a), we generated *ced; dyn-1(n4039)*/+ heterozygous strains and scored the number of persistent cell corpses in *ced; dyn-1(n4039)* homozygous progeny (Experimental Procedures). The Ced phenotypes of the *ced-1* and *ced-6* mutants were only mildly (<14%) enhanced by *dyn-1(n4039)*, while those in the *ced-5*, *ced-10*, or *ced-12* mutants were enhanced by ~50% (Figure 1D). These results suggest that the zygotic activity of *dyn-1* functions in the pathway controlled by *ced-1* and *ced-6*, but not that controlled by *ced-5*, *ced-10*, or *ced-12*.

DYN-1 Clusters on Pseudopods Simultaneously with Phagocytic Receptor CED-1

dyn-1::gfp expressed under P_{dyn-1} or P_{ced-1} is localized to both the cytoplasm and plasma membrane and displays a punctate localization pattern along the apical cell surface (Figure S4, [f]–[i]). In wild-type embryos expressing P_{ced-1} *dyn-1::mrfp1* (monomeric red fluorescence protein 1; Campbell et al., 2002), a bright fluorescent signal is observed on the surface phagocytic cups and phagosomes (Figure 5A). Using embryos that express both P_{ced-1} *ced-1::gfp* and P_{ced-1} *dyn-1::mrfp1* and time-lapse recording (Experimental Procedures), we observed that CED-1::GFP and DYN-1::mRFP1 colocalized simultaneously to extending pseudopods and nascent phagosomes (Figure 5A). The localization of CED-1 and DYN-1 on phagosomes is transient, and CED-1 disappears before DYN-1 does (Figure 5A). The disappearance of CED-1 and DYN-1 occurs long before the complete degradation of dying cells, which takes 60–80 min (Z.Z. unpublished data; see below). These results strongly suggest that DYN-1 and CED-1 work closely in response to an extracellular signal for engulfment.

The Recruitment of DYN-1 to the Site of Engulfment Requires the Functions of *ced-1*, *ced-6*, and *ced-7*, but Not Those of *ced-5*, *ced-10*, or *ced-12*

In *ced* mutant embryos, the localization pattern of DYN-1::GFP on the plasma membrane and in cytoplasm remains unchanged (Figures 5C and 5D). In *ced-5* and *ced-12* mutants, DYN-1::GFP is enriched on those pseudopods that partially surround certain dying cells for a prolonged period of time but fail to fully enclose (Figure 5C), indicating that although the loss of *ced-5* or *ced-12* function blocks the extension of pseudopods, it does not affect the recruitment of DYN-1 to the site of engulfment. In contrast, such partial GFP circles have not been observed in *ced-1*, *-6*, or *-7* mutants, even when the engulfing cell is in contact with the dying cell (Figure 5C, [e] and [f] and data not shown), indicating that the recruitment of DYN-1 to the site of engulfment is defective in these mutants.

We next monitored DYN-1::GFP during phagosome formation in three ventral hypodermal cells, ABplaapppa, ABpraapppa, and ABplaapppp (Williams-Masson et al., 1997), that each engulfs one dying cell (referred to as C1, C2, and C3, respectively) during its extension to the midline of the ventral surface (Figure 5B). In wild-type embryos, the engulfment of C1 and C2 starts at approximately the same time (~330 min after the first cleavage), shortly before that of C3. In *ced-1* embryos, but not in *ced-5* embryos, the removal of these three dying cells is severely delayed or even blocked, indicating that their removal relies primarily on the *ced-1* pathway (Figure S5). We found that in *ced-5*, *-10*, and *-12* mutants, both the dynamics of DYN-1 recruitment and the intensity of the DYN-1::GFP signal around nascent phagosomes are similar to those observed in wild-type embryos (Figures 5D and 5E). However, in *ced-1*, *-6*, and *-7* mutant embryos, the GFP signal intensity around engulfed C1, C2, and C3 is significantly weaker (Figure 5D). In wild-type, *ced-5*, *ced-10*, and *ced-12* mutants, the bright DYN-1::GFP circles remain at least 12 min on enclosed phagosomes (Figures 5A and 5E and data not shown). In *ced-1*, *-6*, and *-7* mutants, the GFP circle remains dim during and after the engulfment process (Figure 5E, [h]–[m] and data not shown). These results indicate that the recruitment of DYN-1 to the site of engulfment requires the function of all three members of the *ced-1* signaling pathway, but neither *ced-5*, *ced-10*, nor *ced-12*. This is consistent with the observation that the zygotic activity of *dyn-1* contributes primarily to the *ced-1* signaling pathway and further suggests that *ced-1*, *-6*, and *-7* all act upstream of *dyn-1*. In *dyn-1(n4039)* embryos, CED-1::GFP is localized to the plasma membrane

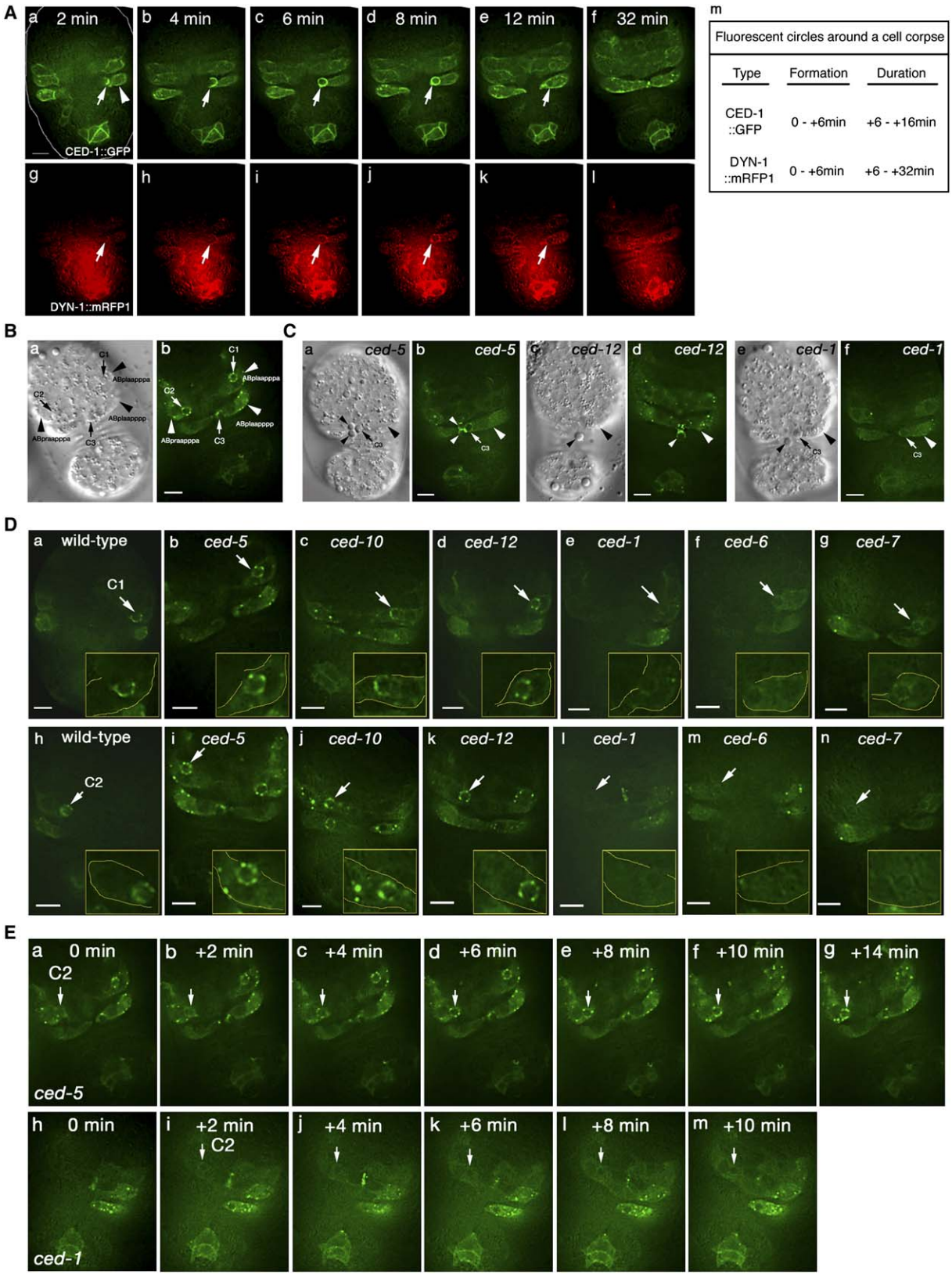

Figure 5. The Recruitment of DYN-1::GFP to the Site of Engulfment Is Defective in *ced-1*, *ced-6*, and *ced-7* Mutants, but Not in *ced-5*, *ced-10*, or *ced-12* Mutants

Epifluorescence images of signals produced by embryos expressing P_{ced-1} *ced-1::gfp*, P_{ced-1} *dyn-1::mrfp1*, and P_{ced-1} *dyn-1::gfp*. Anterior is to the top. Ventral faces readers. The scale bar is 5 μm. All embryos are 330–380 min old.

of engulfing cells and clusters around cell corpses as in wild-type embryos (Supplemental Data and Figure S6).

Abnormal Vesicle Structures Accumulate in *dyn-1*(RNAi)-Engulfing Cells

Intracellular vesicles are known to fuse with engulfing cell membrane at the site of engulfment to provide membrane lipids to the extending pseudopods and to supply digestive enzymes to phagosomes (Booth et al., 2001). We detected various abnormalities related to intracellular vesicles in the gonadal sheath cells of *dyn-1*(RNAi) animals by TEM analysis (Experimental Procedures). In the cytoplasm of wild-type sheath cells, a small number of small vesicles (<100 nm in diameter) were occasionally observed, regardless of whether or not the sheath cell contained a cell corpse (Figure 6A). Occasionally, we observed small vesicles connected to the sheath cell membrane, which may represent exocytic intermediates (Figure 6A, [f]). In the sheath cells of *dyn-1*(RNAi) animals, a large number of intracellular vesicles with abnormal size and morphology were observed. These abnormal vesicles can be grouped into three major classes and are consistent with the well-characterized function of dynamins in vesicle fission as well as with the newly identified role of dynamin in vesicle fusion (Peters et al., 2004). First, very large vesicles, some reaching ~400–700 nm in diameter (Figure 6B, [a]–[c]), accumulate in the cytoplasm of the sheath cells, implying defects in the regulation of vesicle size through fission. These class A vesicles are found at similar frequencies in the sheath cells around engulfed cell corpses, adjacent to unengulfed cell corpses, and adjacent to living germ cells (Figure 6C). Class B abnormal vesicles consist of what appear to be two or more vesicles interconnected via lipid tubules (Figure 6B, [d]–[f]), another possible indication of defects in the fission process. Class C vesicles are those that remain connected to the membrane of phagosomes or phagocytic cups. These incomplete vesicles are much larger than the vesicles found in wild-type animals (Figure 6B, [g]–[i]) and are indicative of defects in efficient vesicle fusion to or fission from the plasma membrane. Unlike class A vesicles, class B and C vesicles are more frequently found in the vicinity of the contact made between sheath cells and cell corpses (Figure 6C) and might represent aberrant intermediate vesicle structures generated and accumulated during the process of cell corpse engulfment and degradation.

Intracellular Vesicles May Be Recruited to Phagocytic Cups and Phagosomes after the Recruitment of CED-1 and DYN-1

One important source of vesicles known to fuse with phagocytic cups and phagosomes is the endosome (Touret et al., 2005). We used a GFP fusion of HGRS-1, the *C. elegans* homolog of human Hrs (hepatocyte growth factor regulated tyrosine kinase substrate), which is an endosomal protein, to track endosomes. When expressed in engulfing cells, an HGRS-1::GFP fusion protein displays a punctate localization pattern in the cytoplasm (Figure 7A) and colocalizes on cytoplasmic puncta with two previously established endosomal markers (Supplemental Data and Figure S7).

In wild-type embryos, cell corpses are surrounded by a strong HGRS-1::GFP signal (Figures 7B and 7C), and time-lapse recording showed that engulfed C1, C2, and C3 were labeled by HGRS-1::GFP circles (Figures 7C–7F). In embryos coexpressing CED-1::GFP and HGRS-1::mRFP1, a very weak signal of HGRS-1::mRFP1 was first visible on CED-1::GFP-labeled pseudopods (Figure 7C, [b], [c], [i], and [j]). The intensity of HGRS-1::mRFP1 gradually increases on the phagosome membrane. Within 20–40 min, the initially punctate mRFP signal evolves to a smooth, continuous circle around the cell corpse (Figure 7C). These observations suggest that endosomes and/or their derivatives are gradually recruited to phagocytic cups and phagosomes. The conversion from puncta to a smooth circle might reflect vesicle incorporation into phagocytic membranes.

Unlike CED-1::GFP, which disappears from the engulfed phagosomes 22 min after phagosome formation (Figures 7C), HGRS-1::mRFP1 continues to associate with phagosomes long after the cell corpse becomes undetectable by DIC microscopy, and likely until it is completely degraded (Figure 7C).

Time-lapse recording of wild-type embryos coexpressing DYN-1::GFP and HGRS-1::mRFP1 indicates that DYN-1 and HGRS-1 are recruited to the same site of engulfment, but with different dynamics. When DYN-1::GFP appeared as a bright circle around engulfed C3, the HGRS-1::mRFP1 circle was very dim (Figure 7D, [a] and [e]). Later, when DYN-1::GFP began to disappear from the phagosomal surface, the intensity of the HGRS-1::mRFP1 signal continued to increase (Figure 7D). Taken together, these observations suggest that endosomes and/or their derivatives are recruited to phagocytic cups and phagosomes, and that the recruitment of HGRS-1-containing vesicles follows that of CED-1 and DYN-1 temporally.

dyn-1 and *ced-1* Mutants Are Defective in the Recruitment of HGRS-1-Containing Vesicles to the Site of Engulfment

In *dyn-1(n4039)*, *ced-1*, *ced-10*, and *ced-12* mutant embryos, the punctate localization pattern of HGRS-1::GFP is similar to that of wild-type embryos (Figure 7F; Movies S1, S2, and S3; data not shown). In some *dyn-1(n4039)*

(A) Time-lapse images of (a–f) CED-1::GFP and (g–l) DYN-1::mRFP1 around the same cell corpse in a wild-type embryo. "0 min," the time point that CED-1::GFP is first detected on the budding pseudopods. Arrows indicate the extending pseudopods. One arrowhead indicates the engulfing cell. (m) Time to form the GFP or mRFP1 circles assayed in (a)–(l) and the duration of these circles.

(B) (a) DIC and (b) GFP fluorescence images of the ventral surface of an embryo indicating the accumulation of DYN-1::GFP on the surface of three cell corpses (arrows) that are engulfed by three hypodermal cells (big arrowheads).

(C) DYN-1::GFP accumulates to the persistent phagocytic cups (small arrowheads) and engulfed C3 cell corpse (arrows) (big arrowheads indicate the engulfing cell) in *ced-5(n1812)* and *ced-12(n3261)* mutant embryos, but not in *ced-1(e1735)* mutant embryos.

(D) The DYN-1::GFP rings around engulfed C1 and C2 in different mutants (*ced-1(e1735)*, *ced-5(n1812)*, *ced-6(n2095)*, *ced-7(n1996)*, *ced-10(n3246)*, and *ced-12(n3261)*). Arrows indicate the engulfed (a–g) C1 and (h–n) C2. The area around each arrow is amplified 1.8-fold and presented in the inset with the engulfing cell boundary highlighted. Images were captured 2–4 min after the full closure of the GFP circle.

(E) Time-lapse images of the DYN-1::GFP circle around an engulfed C2 (arrows) in (a–g) *ced-5(n1812)* and (h–m) *ced-1(e1735)* embryos.

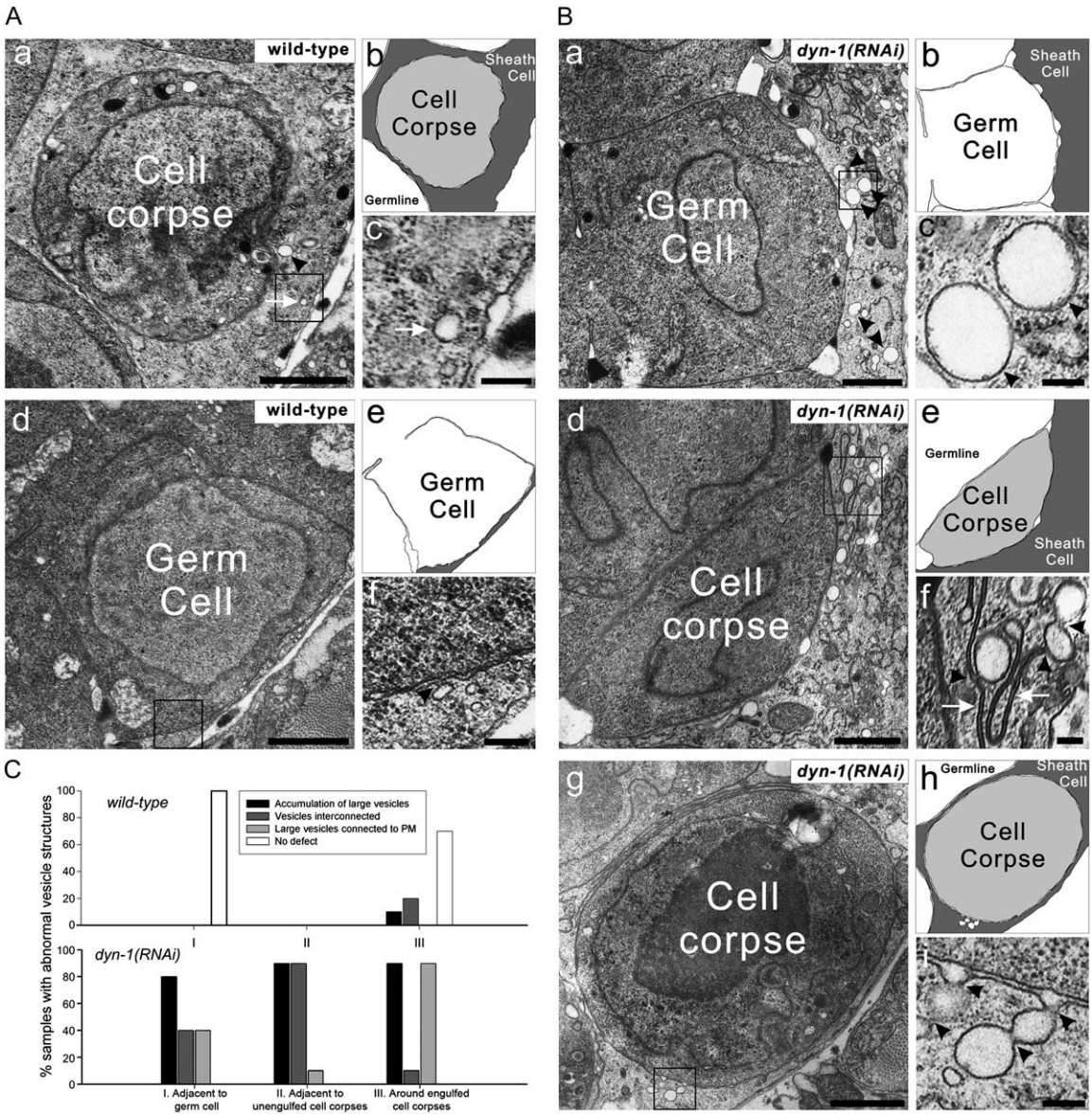

Figure 6. Abnormal Intracellular Vesicles Were Observed in *dyn-1*(RNAi) Animals

(A and B) TEM images of germ cell corpses and their neighboring environment in (A) wild-type and (B) *dyn-1*(RNAi) animals. Regions of sheath cells containing intracellular vesicles (in boxes) are amplified and shown in (A) (panels [c] and [f]) and (B) (panels [c], [f], and [i]). Traces of cell boundaries are shown, with cell identities labeled ([A], panels [b] and [e]; [B], panels [b], [e], and [h]). The scale bar in panels (a) and (d) of (A) and panels (a), (d), and (g) of (B) is 1 μm; the scale bar in panels (c) and (f) of (A) and panels (c), (f), and (i) of (B) is 125 nm. (A) Arrows in (a) and (c) indicate small vesicles. Arrowheads in (a) and (c) indicate large vesicles; in (d) and (f), arrowheads indicate the connection point between small vesicle and the sheath cell membrane. (B) Arrowheads in (a) and (c) indicate large vesicles, arrowheads in (d) and (f) indicate vesicles connected to each other directly or via long lipid tubules (white arrows), and arrowheads in (g) and (i) indicate the connection points between vesicles and sheath cell membranes.

(C) The frequency of occurrence of each class of abnormal vesicular structures. For each cellular context, results are from ten samples from wild-type or *dyn-1*(RNAi) animals.

mutant embryos, C1 and C2 are engulfed despite the overall low engulfment activity. We analyzed the localization of HGRS-1::GFP around C1 and C2 during and after their engulfment. In 64% of the embryos, very little or no GFP signal was detected around C1 and C2 in *dyn-1* embryos (Figures 7E and 7F, [e]) (Movie S3), indicating a defect in the recruitment of HGRS-1(+) vesicles. In the rest of the embryos, bright GFP circles were observed around C1 or C2; however, these circles often remained punctate and failed to convert into smooth circles (Figure 7F, [d]) (Movie S2). These observations suggest multiple defects in the recruitment of HGRS-1(+) vesicles to the phagosome membrane.

We found that in *ced-10* and *ced-12* embryos, as in wild-type embryos, C1 and C2 were labeled with bright GFP circles in every case examined (Figures 7E and 7F), indicating that *ced-10* and *ced-12* do not play a major role in the recruitment of HGRS-1(+) vesicles. In a *ced-1* null mutant background, no circles or very dim circles were observed around C1 and C2 in 75%

of the embryos examined (Figures 7E and 7F, [f]). Thus, the recruitment of HGRS-1(+) vesicles to the site of engulfment requires both the functions of *ced-1* and *dyn-1*, but not the functions of *ced-10* and *ced-12*.

Discussion

A Unique Class of Mutations Revealed a Previously Unknown Function of DYN-1 in the Removal of Apoptotic Cells

C. elegans DYN-1 is involved in synaptic vesicle recycling, receptor-mediated endocytosis of yolk proteins, fluid-phase endocytosis by coelomocytes, and cytokinesis, revealed by the study of the *ky51* mutation and *dyn-1*(RNAi) (Clark et al., 1997; Grant and Hirsh, 1999; Fares and Greenwald, 2001; Thompson et al., 2002). This study describes a previously unidentified role of DYN-1 in the removal of apoptotic cells.

In *dyn-1(n4039)* embryos, the duration of cell corpses is significantly prolonged. *dyn-1*(RNAi) results in defects in both pseudopod extension and the degradation of internalized apoptotic cells. The observations that *dyn-1* acts primarily in engulfing cells for the removal of dying cells; that *dyn-1* functions in a pathway shared by *ced-1*, *-6*, and *-7*, three engulfment-specific genes; and, in particular, that DYN-1::GFP localizes to growing phagocytic cups in a manner dependent on *ced-1*, *ced-6*, and *ced-7* strongly support a direct role of DYN-1 in removing apoptotic cells.

In contrast to the severe defects in the removal of cell corpses, the overall embryonic development proceeds normally until the 4-fold stage in all 14 *dyn-1* alleles we isolated. The number and timing of programmed cell death events remain unchanged in *dyn-1(n4039)* embryos. Furthermore, the uptake of yolk into oocytes and the subsequent redistribution of yolk from other embryonic cell types to intestinal cells are normal in *dyn-1(n4039)* embryos. These observations suggest that the residual activities from the mutant *dyn-1* gene product and from the maternally provided *dyn-1(+)* product are sufficient for many essential cellular processes during early embryogenesis but are insufficient for the clearance of apoptotic cells. In support of this notion, *dyn-1*(RNAi), which presumably knocks down both the maternal and the zygotic gene contributions, results in severe defects in yolk uptake and early embryonic development in addition to the defect in the removal of apoptotic cells (Grant and Hirsh, 1999; this study).

The *dyn-1(ky51)* allele, which severely affects the endocytosis of multiple substances (Clark et al., 1997; Grant and Hirsh, 1999; Fares and Greenwald, 2001), only causes an extremely weak and partially penetrant Ced phenotype. Likewise, the *rme-1* or *rme-8* mutants do not display an obvious Ced phenotype. These observations indicate that defects in endocytosis do not necessarily affect phagocytosis, and that the functions of *dyn-1* in endocytosis and in the removal of apoptotic cells are separable by different mutations (Figure 8).

DYN-1 May Promote the Delivery of Intracellular Vesicles to the Site of Engulfment and Degradation of Apoptotic Cells

During the phagocytosis of opsonized foreign particles by macrophages, the extension of plasma membrane relies on focal exocytosis, the recruitment and subsequent fusion of intracellular vesicles at the site of particle uptake (reviewed by Booth et al., 2001). Quantitative measurements indicate that more than 70% of the phagosome membrane is of endosomal origin (Touret et al., 2005). Similarly, the engulfment of apoptotic cells is likely to require intracellular transport of vesicles to provide sources of membrane lipids at the growing phagocytic cup, although this requirement has not been well studied before.

Electron microscopic images of *dyn-1*(RNAi) animals indicate defects in pseudopod extension around cell corpses. Furthermore, in *dyn-1(n4039)* embryos, the extension of pseudopods around a cell corpse often requires considerably more time to complete; however, the retraction of extending pseudopods from fully embraced cell corpses has not been detected (Supplemental Data and Figure S6). These findings suggest that the primary defect in phagocytosis is unlikely in the fission of phagosomes; rather, it is in the extension of pseudopods. They further raise the possibility that *dyn-1* might act to promote the delivery of vesicles to the phagocytic cup. Consistent with this possibility, we found that DYN-1 mediates the recruitment of HGRS-1(+) vesicles to the site of engulfment.

The apparent inability of *dyn-1* mutants to swiftly degrade internalized cell corpses can also be explained by inefficient delivery of intercellular compartments to phagosomes. The degradation of foreign objects by macrophages relies on the delivery of digestive enzymes via the fusion of endosomes and lysosomes to phagosomes (reviewed by Vieira et al., 2002). We observed a continuing increase of HGRS-1::GFP to the surface of phagosomes after the completion of engulfment, consistent with an additional role of endosomes in the degradation of apoptotic cells. The vesicles delivered to phagocytic cups and phagosomes via *dyn-1* function are likely not limited to HGRS-1(+) compartments. We have observed that a putative lysosomal protein is delivered to phagosomes in a *dyn-1*-dependent manner (X.Y. and Z.Z., unpublished data).

Possible Mechanisms of DYN-1-Mediated Vesicle Delivery

Dynamins in mammals and *Drosophila* are known to form polymers along lipid vesicles and promote the fission of vesicles through GTP hydrolysis (reviewed by Praefcke and McMahon, 2004). Recent studies also implicate dynamin-related proteins in membrane fusion (Peters et al., 2004; reviewed by Praefcke and McMahon, 2004). For example, the vesicle fusion-promoting activity of Vps1, a yeast dynamin-like protein, was identified and attributed to its interaction with components of the membrane fusion t-SNARE complex (Peters et al., 2004).

Interestingly, expression of a dominant-negative form of mammalian dynamin 2, but not dynamin 1, inhibits macrophage phagocytosis, apparently by blocking membrane extension (Gold et al., 1999; Tse et al., 2003). Overexpressed dynamin 2 appears to localize to phagocytic cups (Gold et al., 1999; Di et al., 2003). In addition, antagonizing the function of endogenous dynamin leads to the inhibition of exocytosis in phagocytosing macrophages

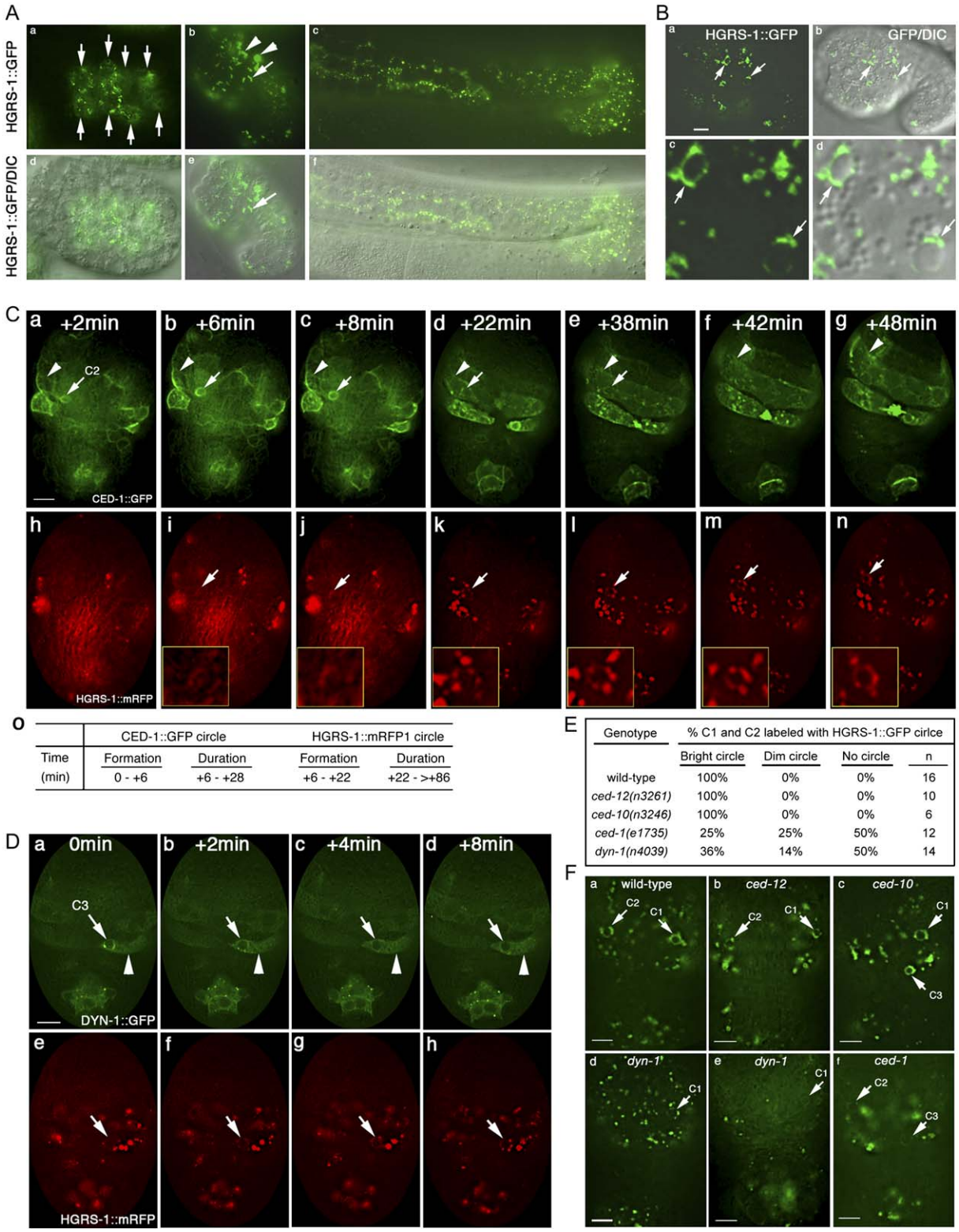

Figure 7. The Endosomal Marker HGRS-1 Clusters around Cell Corpses in a *dyn-1*- and *ced-1*-Dependent Manner

(A–F) All animals are wild-type, except for those shown in (E) and (F) (panels [b]–[e]). Transgenic reporters used are (A, B, and F) P_{ced-1} *hgrs-1::gfp*, (C) P_{ced-1} *ced-1::gfp*, (C and D) P_{ced-1} *hgrs-1::mrfp1*, and (D) P_{ced-1} *dyn-1::gfp*. The scale bars are 5 μm. (A) HGRS-1::GFP in (a) a 200- to 230-min-old embryo, (b) a comma-stage embryo, and (c) the gonad of an adult hermaphrodite; (d), (e), and (f) are the GFP and DIC images of (a), (b), and (c), respectively. Arrows indicate (a) intestinal precursor cells and the (b and e) HGRS-1::GFP signal around one cell corpse. Arrowheads indicates the GFP signal in ventral hypodermal cells. Anterior is to the left. (B) (a) GFP and (b) GFP/DIC merged images of a comma-stage embryo. Arrows indicate cell corpses with a surrounding GFP signal. (c and d) 4-fold amplification to show the same two cell corpses found in (a) and (b) (arrows). Anterior is to the left. (C, D, and F) Epifluorescence images of ~330- to 380-min-old embryos. Anterior is to the top. Ventral faces readers.

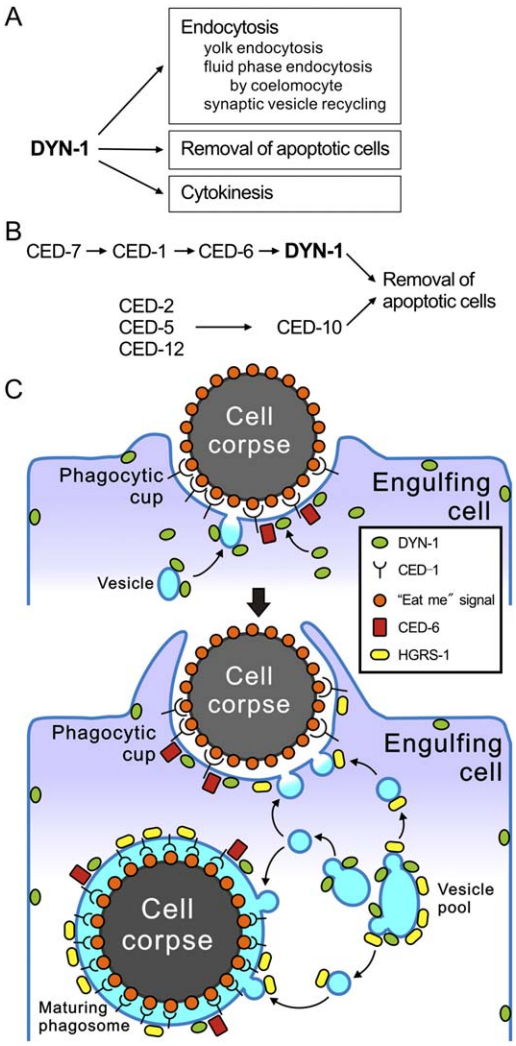

Figure 8. DYN-1 Regulates the Delivery of Vesicles to Phagocytic Cups and Phagosomes in Response to CED-1 Signaling

See text for details.

(A) DYN-1's functions in *C. elegans*.

(B) The position of DYN-1 in the pathways for the removal of apoptotic cells.

(C) Diagram describing how DYN-1 acts to mediate CED-1 signaling. (Upper panel) DYN-1 is recruited to the site of engulfment in response to CED-1 activation. (Lower panel) DYN-1 may act in two distinct steps to promote focal exocytosis: the fission of budding vesicles (HGRS-1-positive or -negative) from an intracellular vesicle pool and the recruitment and fusion of vesicles to their target membranes (phagocytic cup or maturing phagosome).

(Di et al., 2003). However, how dynamin promotes focal exocytosis remains elusive.

Morphologically aberrant vesicles observed in engulfing cells of *dyn-1*(RNAi) animals are consistent with a potential involvement of DYN-1 in both membrane fission and fusion. While abnormally large vesicles and tubular structures suggest defective fission processes, the accumulation of numerous cytoplasmic vesicles and the aberrant membrane structures at the phagocytic cup may be more readily explained by a defect in fusion of vesicles to the plasma membrane. We found that the delivery of HGRS-1(+) vesicles to the growing phagocytic cups and phagosomes was dependent on and preceded by the recruitment of DYN-1 to the same engulfment site. Moreover, in *ced-1* mutant embryos, the lack of DYN-1 localization to the site of engulfment correlates with the defects in recruiting HGRS-1(+) vesicles to the same site. The most straightforward explanation for the above-described result is that the recruitment of DYN-1 promotes fusion of endosomes or endosome-derived vesicles at their destination. Together, the above-described observations implicate that DYN-1 may regulate the focal exocytosis of intracellular vesicles by using its putative fission and fusion activities (Figure 8).

DYN-1 May Mediate the Signaling of Phagocytic Receptor CED-1

Genetic analyses suggest that *dyn-1* acts in the same genetic pathway as *ced-1*, *-6*, and *-7*. In addition, the functions of these three genes are required for the recruitment of DYN-1 to the extending pseudopods. In *ced-1* mutant embryos, the removal of three cell corpses (C1, C2, C3) is severely delayed, correlating with the defect in the recruitment of DYN-1 and the HGRS-1(+) vesicles to the site of engulfment. These results suggest that the activation of CED-1 in response to the extracellular "eat me" signal marks the site of phagosome formation and promotes the recruitment of DYN-1 to this site (Figure 8). To our knowledge, we have thus identified a novel cellular event regulated by CED-1: the delivery of intracellular vesicles to extending pseudopods and phagosomes.

How CED-1 recruits and activates DYN-1 is not known. CED-6, a PTB domain protein and a candidate adaptor for CED-1, is required for the recruitment of DYN-1, suggesting that CED-6 or an unidentified CED-6-interacting protein in the CED-1 complex may mediate the interaction of DYN-1 with activated CED-1. The localization of DYN-1 to the site of engulfment is transient and signal dependent. It is plausible that the posttranslational modification of CED-1, CED-6, and/or DYN-1 as well as other proteins in the CED-1 complex triggers or stabilizes the interactions among these proteins. Alternatively, specific phosphoinositides enriched on the surface of phagocytic cups and phagosomes (Vieira et al., 2002) may promote the recruitment of DYN-1 and other effectors of engulfment. DYN-1 possesses a PH domain that could associate with phosphoinositides. While the ABC transporter CED-7, whose functions are required in both dying and engulfing cells, is likely to regulate DYN-1 by activating CED-1 (Zhou et al., 2001b), it may

(C) Coexpressed (a–g) CED-1::GFP and (h–n) HGRS-1::mRFP1 signals around cell corpse C2 (arrows) during and after it is engulfed by ABpraapppa (arrowheads). 0 min, the moment that pseudopods (visible with CED-1::GFP) start to extend around C2. The insets in (i)–(n) represent 2.6-fold amplified images of the region indicated by arrows. (o) The time needed to form GFP and mRFP1 circles around C2, as assayed in (a)–(n), and the duration of the circles. (D) Images of (a–d) DYN-1::GFP and (e–h) HGRS-1::mRFP around cell corpse C3 (arrows) at different times after it is engulfed by ABplaapppp (arrowheads). (E) The frequency that the HGRS-1::GFP circles are detected around C1 and C2 in different genetic backgrounds. n, the number of C1 and C2 analyzed. (F) HGRS-1::GFP signal in embryos of different genetic backgrounds. Arrows indicate the engulfed C1, C2, and C3.

also influence the local composition of phospholipids at the site of engulfment.

Recently, *ced-10* was proposed to act downstream of *ced-1* at a convergence point of the *ced-1* and *ced-5* pathways to regulate cytoskeletal reorganization during engulfment (Kinchen et al., 2005). We found that the zygotic *dyn-1* activity is in parallel to the engulfment pathway controlled by *ced-5*, *-10*, and *-12*. In addition, neither *ced-5*, *ced-10*, nor *ced-12* is required for the proper recruitment of DYN-1 to the site of engulfment. Furthermore, the *dyn-1*-dependent recruitment of HGRS-1(+) vesicles does not require *ced-10* or *ced-12*. These observations suggest that neither CED-5, CED-10, nor CED-12 plays a detectable role in recruiting DYN-1 or controlling focal exocytosis.

The Function of Dynamins in the Removal of Apoptotic Cells May Be Conserved from *C. elegans* to Mammals

Although a dominant-negative form of mammalian dynamin 2 was reported to affect macrophage phagocytosis of foreign objects (Gold et al., 1999), the in vivo function of dynamin in phagocytosis has not been demonstrated with genetic mutations before. Furthermore, the requirement of dynamin in the clearance of apoptotic cells has not been reported. In mammals, apoptotic cells are recognized by specialized macrophage receptors distinct from those recognizing foreign pathogens; in addition, internalized apoptotic cells elicit a profoundly different response compared to that elicited by internalized foreign particles (reviewed by Savill and Fadok, 2000). Our finding that human dynamin 2 can partially rescue the Ced phenotype displayed by *dyn-1* mutants indicates that DYN-1 is a functional counterpart of human dynamins and suggests that particular mammalian dynamins may mediate the action of specific phagocytic receptors to promote the clearance of apoptotic cells. Understanding this particular role of dynamin will shed light on how vesicle trafficking events are regulated by phagocytic receptors and how the human immune system elicits distinct responses to apoptotic cells and foreign pathogens.

Experimental Procedures

Mutations and Strains

C. elegans strains were grown at 20°C as previously described (Brenner, 1974). The N2 Bristol strain was used as the reference wild-type strain. Mutations and integrated transgenes used are described by Riddle et al. (1997), except where noted otherwise: LGI, *ced-1(e1735, n1506)*, *ced-12(n3261)* (Zhou et al., 2001a), *sem-4(n1378)*, *unc-75(e950)*; LGIII, *dpy-17(e164)*, *unc-36(e251)*, *ced-6(n2095)*, *ced-7(n1996)*; LGIV, *dpy-20(e1282)*, *dpy-9(e12)*, *ced-2(e1752)*, *ced-5(n1812)*; LGV, *unc-76(e911)*; LGX, *enIs2* (this work), *unc-3(e151)*, *lin-15(n765)*, *dyn-1(n4335, n4098, n4334, n4332, n4039, n4333, en40, en34, en15, en7, en37, en41, en12, en9)* (this work), *dyn-1(ky51)* (Clark et al., 1997), *dyn-1(tm852)* (S. Mitani, personal communication). To generate double mutants with *dyn-1(n4039)* and *ced-1*, *-5*, *-6*, *-10*, and *-12*, we first generated *ced; enIs2* (*enIs2* is an integrated *gfp* reporter on the X chromosome) strains. We crossed *ced; enIs2* males into *sem-4(n1378); n4039/enIs2* animals, and we isolated *ced; n4039/enIs2* animals in F2 progeny.

Time-Lapse Recording with DIC Microscopy

A Zeiss Axioplan 2 compound microscope equipped with Nomarski DIC accessories, an AxioCam camera, and AxioVision imaging software was used. For each time point, 40 serial z sections at 0.5 μm/section were recorded. To detect the occurrence of cell death events, 160-min-old embryos (embryos at ~160 min past the first cleavage) were recorded for 300 min in 3 min intervals, and the time point at which every cell corpse first appeared was identified. To measure the duration of cell corpses, recording started when an embryo was at 352 min of age and ended after 80 min, with 3 min intervals. Cell corpses appearing between 352 and 376 min were followed. To observe embryonic development, one-cell embryos isolated from dissected mothers were recorded for 810 min at 5 min intervals. Embryonic stages were determined as previously described (Sulston et al., 1983) with slight modification. In brief, 1.5-, 2-, and 3-fold stages were defined as embryos whose body lengths were 1.5, 2, and 3 times, respectively, the length of an egg. We define early 4-fold and late 4-fold stages as embryos whose bodies make three turns and contain nascent and fully developed grinders, respectively.

Fluorescence Microscopy

An Olympus IX70-Applied Precision DeltaVision microscope equipped with a Photometris Coolsnap digital camera and Applied Precision Softworx software was used. For each embryo, 40 serial z sections with 0.5 μm intervals were captured and deconvolved. To record the localization of GFP or mRFP1 during embryogenesis, 300- to 330-min-old embryos were used. Recording occured in 2 min intervals. Signs of progressive embryonic development, such as the extension of ventral hypodermal cells and the turning of the embryos, were examined to ensure that data were collected from embryos developing normally.

Transmission Electron Microscopy

Samples of adult hermaphrodite gonads were prepared and analyzed as previously described (Zhou et al., 2001b). We analyzed germ cell corpses in each gonad arm. To determine whether each cell corpse was engulfed, we analyzed a series of 50 nm sections that covered the entire length of the cell corpse and observed whether the cell corpse was fully enclosed inside the gonadal sheath cell (Figure S3). To analyze the number and morphology of vesicles in gonadal sheath cells, we examined the sheath cell plasma membrane and cytoplasm in regions within 1 μm of living germ cells, unengulfed cell corpses, or engulfed cell corpses. Ten samples were analyzed for each specified region. For each sample, five consecutive sections were analyzed.

Supplemental Data

Supplemental Data include information on mapping and cloning of *n4039*, *dyn-1* RNAi, construction of *dyn-1* plasmids, and identification of *dyn-1* alleles and their molecular lesions and are available at http://www.developmentalcell.com/cgi/content/full/10/6/743/DC1/.

Acknowledgments

We thank H.R. Horvitz, in whose laboratory this project was initiated; E. Hartwieg for help with TEM; B. Grant for helpful suggestions; A. Fire, A. Coulson, B. Grant, R. Tsien, S. Mitani, and the *Caenorhabditis* Genetics Center for reagents; X. He for the DeltaVision; and H. Schwartz, T. Shin, A. Kuspa, X. He, A. Antebi, H. Bellen, and members of the Zhou lab, particularly R. Edlund and P. Mangahas, for helpful comments. Z.Z. is supported by the National Institutes of Health (GM067848), the Cancer Research Institute, and the March of Dimes Foundation.

Received: June 24, 2005
Revised: February 20, 2006
Accepted: April 5, 2006
Published: June 5, 2006

References

Booth, J.W., Trimble, W.S., and Grinstein, S. (2001). Membrane dynamics in phagocytosis. Semin. Immunol. *13*, 357–364.

Bossinger, O., and Schierenberg, E. (1996). The use of fluorescent marker dyes for studying intercellular communication in nematode embryos. Int. J. Dev. Biol. *40*, 431–439.

Brenner, S. (1974). The genetics of *Caenorhabditis elegans*. Genetics *77*, 71–94.

Campbell, R.E., Tour, O., Palmer, A.E., Steinbach, P.A., Baird, G.S., Zacharias, D.A., and Tsien, R.Y. (2002). A monomeric red fluorescent protein. Proc. Natl. Acad. Sci. USA *99*, 7877–7882.

Clark, S.G., Shurland, D.L., Meyerowitz, E.M., Bargmann, C.I., and van der Bliek, A.M. (1997). A dynamin GTPase mutation causes a rapid and reversible temperature-inducible locomotion defect in *C. elegans*. Proc. Natl. Acad. Sci. USA *94*, 10438–10443.

Di, A., Nelson, D.J., Bindokas, V., Brown, M.E., Libunao, F., and Palfrey, H.C. (2003). Dynamin regulates focal exocytosis in phagocytosing macrophages. Mol. Biol. Cell *14*, 2016–2028.

Ellis, R.E., Jacobson, D.M., and Horvitz, H.R. (1991). Genes required for the engulfment of cell corpses during programmed cell death in *Caenorhabditis elegans*. Genetics *129*, 79–94.

Fares, H., and Greenwald, I. (2001). Genetic analysis of endocytosis in *Caenorhabditis elegans*: coelomocyte uptake defective mutants. Genetics *159*, 133–145.

Gold, E.S., Underhill, D.M., Morrissette, N.S., Guo, J., McNiven, M.A., and Aderem, A. (1999). Dynamin 2 is required for phagocytosis in macrophages. J. Exp. Med. *190*, 1849–1856.

Grant, B., and Hirsh, D. (1999). Receptor-mediated endocytosis in the *Caenorhabditis elegans* oocyte. Mol. Biol. Cell *10*, 4311–4326.

Grant, B., Zhang, Y., Paupard, M.C., Lin, S.X., Hall, D.H., and Hirsh, D. (2001). Evidence that RME-1, a conserved *C. elegans* EH-domain protein, functions in endocytic recycling. Nat. Cell Biol. *3*, 573–579.

Gumienny, T.L., Lambie, E., Hartwieg, E., Horvitz, H.R., and Hengartner, M.O. (1999). Genetic control of programmed cell death in the *Caenorhabditis elegans* hermaphrodite germline. Development *126*, 1011–1022.

Hinshaw, J.E. (2000). Dynamin and its role in membrane fission. Annu. Rev. Cell Dev. Biol. *16*, 483–519.

Kinchen, J.M., Cabello, J., Klingele, D., Wong, K., Feichtinger, R., Schnabel, H., Schnabel, R., and Hengartner, M.O. (2005). Two pathways converge at CED-10 to mediate actin rearrangement and corpse removal in *C. elegans*. Nature *434*, 93–99.

Labrousse, A.M., Shurland, D.L., and van der Bliek, A.M. (1998). Contribution of the GTPase domain to the subcellular localization of dynamin in the nematode *Caenorhabditis elegans*. Mol. Biol. Cell *9*, 3227–3239.

Liu, Q.A., and Hengartner, M.O. (1998). Candidate adaptor protein CED-6 promotes the engulfment of apoptotic cells in *C. elegans*. Cell *93*, 961–972.

Lundquist, E.A., Reddien, P.W., Hartwieg, E., Horvitz, H.R., and Bargmann, C.I. (2001). Three *C. elegans* Rac proteins and several alternative Rac regulators control axon guidance, cell migration and apoptotic cell phagocytosis. Development *128*, 4475–4488.

Mangahas, P.M., and Zhou, Z. (2005). Clearance of apoptotic cells in *Caenorhabditis elegans*. Semin. Cell Dev. Biol. *16*, 295–306.

Niemann, H.H., Knetsch, M.L., Scherer, A., Manstein, D.J., and Kull, F.J. (2001). Crystal structure of a dynamin GTPase domain in both nucleotide-free and GDP-bound forms. EMBO J. *20*, 5813–5821.

Peters, C., Baars, T.L., Buhler, S., and Mayer, A. (2004). Mutual control of membrane fission and fusion proteins. Cell *119*, 667–678.

Praefcke, G.J., and McMahon, H.T. (2004). The dynamin superfamily: universal membrane tubulation and fission molecules? Nat. Rev. Mol. Cell Biol. *5*, 133–147.

Reddien, P.W., and Horvitz, H.R. (2000). CED-2/CrkII and CED-10/Rac control phagocytosis and cell migration in *Caenorhabditis elegans*. Nat. Cell Biol. *2*, 131–136.

Reddien, P.W., and Horvitz, H.R. (2004). The engulfment process of programmed cell death in *Caenorhabditis elegans*. Annu. Rev. Cell Dev. Biol. *20*, 193–221.

Riddle, D.L., Blumenthal, T., Meyer, B.J., and Priess, J.R. (1997). *C. elegans* II (Plainview, NY: Cold Spring Harbor Laboratory Press).

Savill, J., and Fadok, V. (2000). Corpse clearance defines the meaning of cell death. Nature *407*, 784–788.

Su, H.P., Nakada-Tsukui, K., Tosello-Trampont, A.C., Li, Y., Bu, G., Henson, P.M., and Ravichandran, K.S. (2002). Interaction of CED-6/GULP, an adapter protein involved in engulfment of apoptotic cells with CED-1 and CD91/low density lipoprotein receptor-related protein (LRP). J. Biol. Chem. *277*, 11772–11779.

Sulston, J.E., and Horvitz, H.R. (1977). Post-embryonic cell lineages of the nematode, *Caenorhabditis elegans*. Dev. Biol. *56*, 110–156.

Sulston, J.E., Schierenberg, E., White, J.G., and Thomson, N. (1983). The embryonic cell lineage of the nematode *Caenorhabditis elegans*. Dev. Biol. *100*, 64–119.

Thompson, H.M., Skop, A.R., Euteneuer, U., Meyer, B.J., and McNiven, M.A. (2002). The large GTPase dynamin associates with the spindle midzone and is required for cytokinesis. Curr. Biol. *12*, 2111–2117.

Touret, N., Paroutis, P., Terebiznik, M., Harrison, R.E., Trombetta, S., Pypaert, M., Chow, A., Jiang, A., Shaw, J., Yip, C., et al. (2005). Quantitative and dynamic assessment of the contribution of the ER to phagosome formation. Cell *123*, 157–170.

Tse, S.M., Furuya, W., Gold, E., Schreiber, A.D., Sandvig, K., Inman, R.D., and Grinstein, S. (2003). Differential role of actin, clathrin, and dynamin in Fc gamma receptor-mediated endocytosis and phagocytosis. J. Biol. Chem. *278*, 3331–3338.

Vieira, O.V., Botelho, R.J., and Grinstein, S. (2002). Phagosome maturation: aging gracefully. Biochem. J. *366*, 689–704.

Williams-Masson, E.M., Malik, A.N., and Hardin, J. (1997). An actin-mediated two-step mechanism is required for ventral enclosure of the *C. elegans* hypodermis. Development *124*, 2889–2901.

Wu, Y., and Horvitz, H.R. (1998a). The *C. elegans* cell corpse engulfment gene *ced-7* encodes a protein similar to ABC transporters. Cell *93*, 951–960.

Wu, Y., and Horvitz, H.R. (1998b). *C. elegans* phagocytosis and cell-migration protein CED-5 is similar to human DOCK180. Nature *392*, 501–504.

Yuan, J., Shaham, S., Ledoux, S., Ellis, H.M., and Horvitz, H.R. (1993). The *C. elegans* cell death gene *ced-3* encodes a protein similar to mammalian interleukin-1 beta-converting enzyme. Cell *75*, 641–652.

Zhang, Y., Grant, B., and Hirsh, D. (2001). RME-8, a conserved J-domain protein, is required for endocytosis in *Caenorhabditis elegans*. Mol. Biol. Cell *12*, 2011–2021.

Zhou, Z., Caron, E., Hartwieg, E., Hall, A., and Horvitz, H.R. (2001a). The *C. elegans* PH domain protein CED-12 regulates cytoskeletal reorganization via a Rho/Rac GTPase signaling pathway. Dev. Cell *1*, 477–489.

Zhou, Z., Hartwieg, E., and Horvitz, H.R. (2001b). CED-1 is a transmembrane receptor that mediates cell corpse engulfment in *C. elegans*. Cell *104*, 43–56.

Zhou, Z., Mangahas, P.M., and Yu, X. (2004). The genetics of hiding the corpse: engulfment and degradation of apoptotic cells in *C. elegans* and *D. melanogaster*. Curr. Top. Dev. Biol. *63*, 91–143.